Defence Science Journal, Vol. 65, No. 2, March 2015, pp. 99-106, DOI : 10.14429/dsj.65.7147

Slag Prediction in Submerged Rocket Nozzle Through Two-Phase CFD Simulations

Amit Kumar Chaturvedi[*], Sudarshan Kumar[#], and Debasis Chakraborty[!]

[*]*Advanced Systems Laboratory, Hyderabad - 500 058, India*
[#]*Indian Institute of Technology Bombay, Mumbai - 400 076, India*
[!]*Defence Research and Development Laboratories, Hyderabad - 500 005, India*
[!]*E-mail:debasis_cfd@drdl.drdo.in*

ABSTRACT

A computational procedure has been established to predict the slag in a practical solid rocket motor with submerged nozzle. Both single-phase and two-phase flow analyses have been performed in the rocket motor port. Three-dimensional Navier-Stokes equations along with SST turbulence model have been solved for gas-phase calculations. The effect of ejected alumina particles from the propellant geometry on the flow field has been simulated through Lagrangian tracking method. The computational methodology is firstly validated by comparing against other numerical results of rocket motors available in the literature before applying the same to predict the slag accumulation of a submerged rocket motor for strategic applications. Burn-back geometries at different instants have been simulated and parametric studies were performed to find out the effect of Al_2O_3 particle size. It was observed that the slag capture rate increases uniformly with $A1_2O_3$ particle size. The predicted slag accumulation data match closely with the ground test data for the range of conditions simulated in the present work.

Keywords: Slag prediction, submerged rocket nozzle, CFD simulation, solid rocket motor, rocket motor performance, nozzle erosion

1. INTRODUCTION

Many solid rockets use aluminized propellants and submerged nozzles to improve their overall performance. During propellant burning, the aluminum powder melts to form agglomerates on the propellant surface. These agglomerates either stream along the surface and onto the case wall, or are ejected into the highly rotational core flow where these burn almost completely. Slag is generated when the wall streaming or gas field-driven particles get trapped behind the submerged nozzle. The accumulated slag is a dead weight and is detrimental to the motor performance. The schematic of the aft section of a typical submerged nozzle is shown in Fig. 1. The toroidal shaped volume around the nozzle nose tip acts as a catchment area that entraps burning aluminum particles in the aft end of the solid rocket motor (SRM). This entrapment occurs either by impingement on some portions of the back-face of the nozzle, or through a capture in a recirculation zone.

The aft dome flow-field of a solid rocket motor has a significant impact on the operation of the motor as well as its performance. The pressure distribution in this region influences the design requirements of the nozzle-to-case joint, and the shear layer structure determines the heat transfer rates, and thus determines the requirements of the liner design. The interactions between the particulate phases and the nozzle inlet section determines the slag accumulation rate and thus affects the nozzle erosion and motor performance. Because of the importance of accurate prediction of accumulated slag in the rocket motor, the problem has been investigated by many researchers over the past few decades, both experimentally and numerically. During the main burn phase, exhaust particles were collected in numerous, high-altitude samplings and ground tests are well documented in the literature[1-4].

Salita[5,6] and Cesco[7] , *et al.* have given a detailed overview of issues and problems of slag accumulation prediction methods. However, lack of good data of Al_2O_3 particle size distributions in the chamber and erroneous use of potential flow modelling of viscous dominated flows have led to improper conclusions on slag accumulation which adversely affects the design of solid rocket motors in yester years. With proper mathematical characterisation of quench-bomb test results, analyses of real-time X-ray radiography (RTR) of slag accumulation history in full-scale motors, and use of

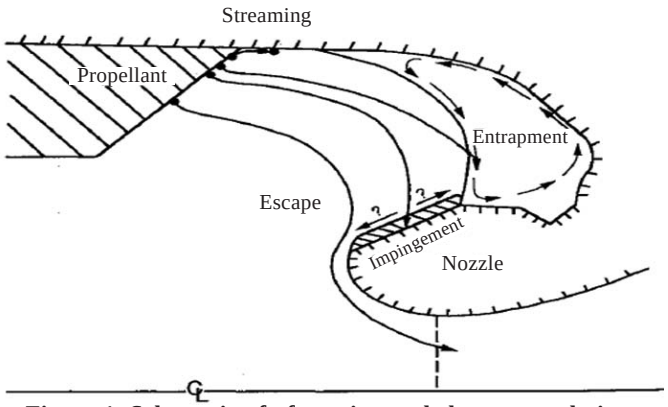

Figure 1. Schematic of aft station and slag accumulation.

Received 9 May 2014, revised 11 February 2015, online published 21 April 2015

two-phase viscous flow solvers have improved the prediction methodologies significantly. Roseband and Gany[8] have demonstrated that aluminium particles coated with nickel reduces agglomeration compared to uncoated aluminium particles and remain in powder form while improving its ignitability. Sippel[9], *et al*. replaced aluminum powder of a composite solid propellant with fuel-rich, mechanically activated composite particles (aluminum/polytetrafluoroethylene, Al/PTFE 90/10 and 70/30 wt.%) and observed 66 per cent decrease in agglomerate diameter compared to agglomerates formed from reference spherical aluminum. Smaller diameter condensed phase products and more gaseous products decrease two-phase flow loss and reduce slag accumulation.

Simulation of solid-propellant rocket motors from first principles with minimal empirical modelling is a challenging task. However, with the advent of powerful computers, robust numerical algorithms, computational fluid dynamics (CFD) tools are increasingly being used to simulate the flow-field of the solid rocket motor and to evaluate the slag accumulation. The presence of the cavity in the vicinity of the submerged nozzle region makes the flow-field complex. The flow in the aft-dome chamber is turbulent, whereas the flow in the cavity is laminar with possible recirculation regions[5,6]. Previous calculation methodologies[10-12] involve use of inviscid methods with boundary-layer corrections to the mean flow. In recent works, numerical solutions[13-16] of the Reynolds-averaged Navier-Stokes equations along with turbulence models have been reported. The motion of the particles is described in the Lagrangian reference frame where the position, velocity vectors, size, temperature, etc. of the particle are updated along the trajectories in the computational space. The two-phase flow is simulated by combining the solution of the gas phase including the inter-phase coupling terms for the continuous phase with the Lagrangian description for the particulate phase.Wirzbergeret[15] *et al*. have presented a model for slag accumulation from the calculation of two-phase viscous flow inside the solid rocket motor port. Najjar[16], *et al*. simulated the flow-field in AFRL 70-lb BATES and RSRM motors at several time instances in the burn time using a multiphase viscous solver in unstructured mesh and a parallel particle localisation algorithm.

In the present study, slag accumulation in a solid rocket motor is predicted using a general purpose CFD code[17]. Both single-phase and two-phase flow calculations were carried out in the rocket motor port and the calculation methodologies were validated against literature results. The validated methodology was applied to predict the slag accumulation of a practical rocket motor of a strategic system. Parametric studies were carried out to understand the effects of different particle sizes on the slag deposition and the computed results were compared with the static test data.

2. COMPUTATIONAL DETAILS

Three-dimensional RANS equations were solved for density, velocity components, and temperature using a general purpose CFD code Ansys (Fluent)[17]. A cell-centered finite-volume method based on the linear reconstruction scheme that allows use of computational elements with arbitrary polyhedral topology, including quadrilateral, hexahedral, triangular, tetrahedral, pyramidal, prismatic and hybrid meshes. Second-order Roe scheme was used for spatial discretisation of the inviscid fluxes whereas diffusion terms were discretised using a second-order central differencing scheme. Temporal terms were discretized through a first-order scheme. The discretised algebraic equations were solved using a point-implicit linear equation solver (ILU factorization scheme on a symmetric block Gauss-Seidel) in conjunction with an algebraic multi-grid (AMG) method to accelerate solution convergence. Shear stress transport model[18] was employed for turbulence closure. Fourier's law for heat conduction was used to calculate heat flux.

The trajectory of a discrete phase particle can be predicted by integrating the particle momentum equation, which is written in a Lagrangian reference frame as:

$$\frac{dv_p}{dt} = \frac{3\rho_g C_d \left|\bar{v}_g - \bar{v}_p\right| (\bar{v}_g - \bar{v}_p)}{4\rho_p D} + \bar{g} \quad (1)$$

where ρ_g, ρ_p, v_g, v_p are the gas and particle densities and velocities, respectively, g is acceleration due to gravity, D is the droplet diameter, and C_d is drag coefficient for spherical droplet and calculated from the following correlation:

$$C_d = \frac{24}{\mathrm{Re}_p}(1 + 0.15\,\mathrm{Re}_p^{0.687}) \quad \mathrm{Re_p} < 1000 \quad (2)$$

$$C_d = 0.438 \quad \mathrm{Re_p} > 1000 \quad (3)$$

$\mathrm{Re_p}$ is the relative Reynolds number, which is defined as

$$\mathrm{Re}_p = \frac{\rho_p D \left|v_g - v_p\right|}{\mu} \quad (4)$$

Constant mass flow inlet condition with mass flow rate normal to the boundary surface is applied at the propellant grain surface and the inflow boundary. Initial pressure, calculated from the pressure time history and constant temperature was applied. A pressure outlet-based boundary condition was applied at the exit plane. No slip wall boundary condition was applied at all walls. The solution is considered to be converged when RMS residuals of the flow and energy balance of the system are of the order of 10^{-5} and 10^{-6}, respectively.

3. RESULTS AND DISCUSSIONS

3.1 Single-Phase Calculation of Titan IV SRMU Flow Field

The Titan IV SRMU[19,20] is a 3.2 m diameter and 34.14 m long three-segment motor with graphite epoxy composite case. The motor is loaded with 312.37 ton of composite propellant comprising 12 per cent Hydroxyl-terminated polybutadiene (HTPB) as binder, 69 per cent ammonium perchlorate (AP) and, 19 per cent aluminum. The nozzle has a composite elastomer flex seal with a maximum 6° gimbal.

The propellant burn-backs for the Titan IV SRMU at 0s, 50s, and 100 s after ignition were taken as given by Mentor[18] and reproduced in Fig. 2. The internal geometry has been divided into 11 blocks to generate computational grid. The quadrilateral cells for 0s, 50s, and 100s areof sizes 0,33 mm, 0.35 mm, and 0.39 mm, respectively. Simulations

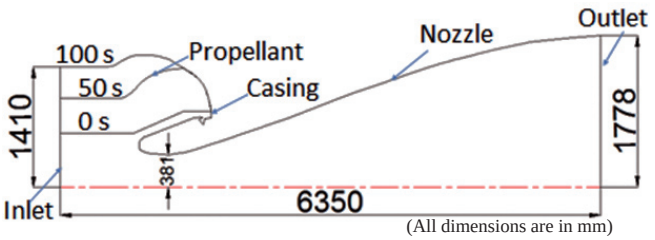

Figure 2. Titan IV SRMU nozzle, motor, and propellant burn-backs at 0, 50, and 100 s (reproduced[19]).

were carried out by varying the grids starting from 20.34 mm to 2.159 mm with varying minimum grid size and the results are found to be independent of grid size as can be seen in the centre line pressure distribution along the nozzle axis presented in Fig 3.Grid convergence or discretisation error, which is the error of the solution of the different equations compared to the exact solution of the partial differential equation, is the major source of numerical error. Introduced by Roache[21], the formulation was used by Aswin and Chakraborty[22] and Manna[23], *et al.* to estimate the error for the problems of sonic jet injection into supersonic cross-stream and scramjet combustor flow-field simulation, respectively.

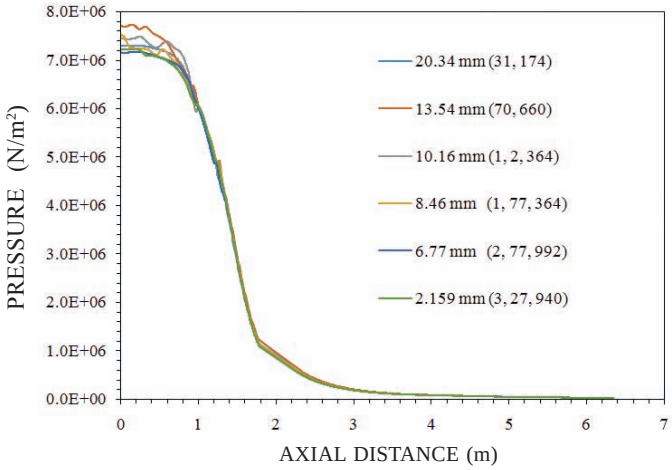

Figure 3. Comparison of centreline pressure distribution with different grids.

The grid convergence index (GCI) is defined as

$$GCI = F_s \frac{1\varepsilon 1}{(h_2 / h_1)^p - 1}, \qquad \varepsilon = (f_2 - f_1)/f_1 \tag{5}$$

where f represent any parameter and the indices 1 and 2 refer to the fine and coarse grid solutions; h, p and F_s are the order of grid spacing and accuracy of numerical scheme, and factor of safety, respectively. For h_2/h_1 =2, p=2 and F_s=3, the GCI of present problem is 0.28 per cent, indicating that all the solutions presented in this paper are independent of the grid size chosen for the simulations.

The qualitative features of the flow-field in the motor port at three different time instants are shown through the distribution of Mach number in Fig. 4. All the flow features in the motor port including low-speed region near the cavity and high-speed region in the nozzle portion is clearly visible in the figure. To depict the flow features in the cavity region, the blown up view of the streamlines is shown in Fig. 5. The recirculation

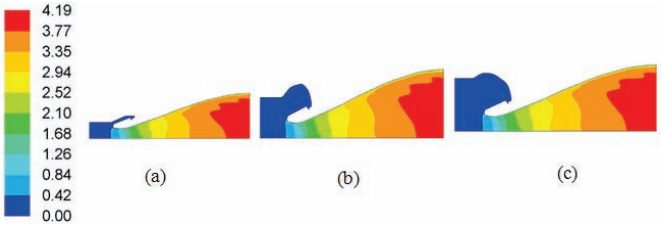

Figure 4. Mach number contour plot for (a) 0 s, (b) 50 s, and (c) 100 s.

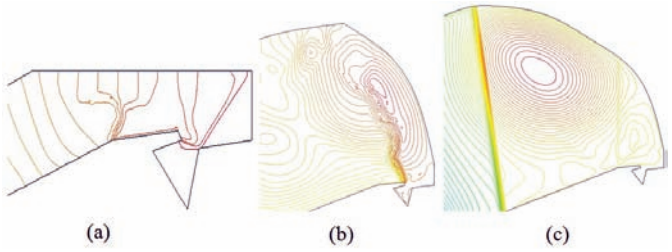

Figure 5. Streamlines in the motor cavity for: (a) 0 s, (b) 50 s, and (c) 100 s, respectively.

region is clearly visible in the cavity region due to which the alumina particles are trapped and result in slag accumulation. The recirculation bubble in the cavity has changed its size and shape as the time progresses. The centreline Mach number and pressure (p/p_0) for different burn-back geometries were compared with numerical results[20] in Fig. 5 and a good match has been obtained.

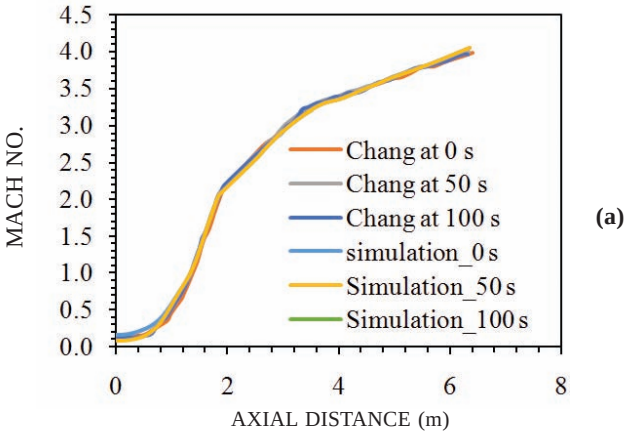

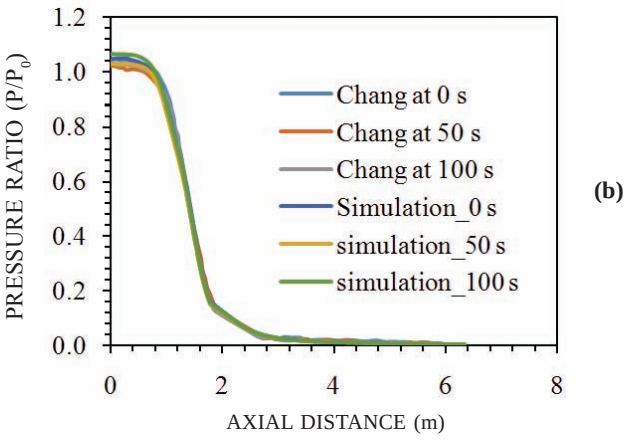

Figure 6. Comparison of centreline: (a) Mach number, (b) pressure distribution with other numerical results.

3.2 Two-phase Flow Calculation (Comparison with Space Shuttle RSRM)

The burn-back configuration of space shuttle RSRM at 19s is taken as given by Madabhushi[24], *et al.* is reproduced in Fig. 7. At 0s, the propellant grain surface lies below the nozzle entrance (lip) whereas for the t = 19s burn-back configuration, the grain surface lies above the nozzle entrance. Thus the particles in the chamber core as well as those close to the walls are unlikely to enter the submerged nozzle cavity for the initial time grain configuration, whereas for the 19-s burn-back configuration, some of the particles are likely to accumulate in the cavity.

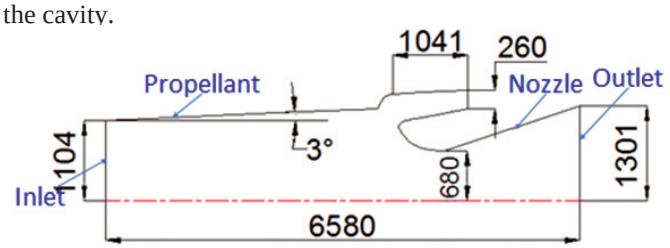

Figure 7. Schematic geometry for 19-s burn-back configuration[24].

The internal geometry has been divided into 9 blocks and 0.22 mm quadrilateral cells were used to generate the grid. The propellant burning rate was assumed to be 19.28 kg/m^{2}s and the nominal chamber pressure and gas temperature were assumed to be 4.83 MPa and 3400 K, respectively. For two-phase calculations, the particulate phase was injected at the propellant surface and the inflow boundary. In the present study, the $A1_2O_3$ smoke was included with the continuous phase, and the particulate phase was assumed to consist only of $A1_2O_3$ agglomerates. The mass density of the particles was assumed to be 2200 kg/m^3.The particle injection velocity was assumed to be 75 per cent of the local gas velocity.

The computed Mach number distribution for the single-phase and two-phase flows near the nozzle region is compared with the results of Madabushi[24], *et al.* in Fig. 8(a) and 8(b), respectively. The two-phase flow simulation has been carried out with particulate phase of 150 µm particle size along with the continuous gas phase. A good qualitative match has been obtained between the two cases, as shown in the figure. The comparison of the present computations between single-phase flow and the two-phase flow are presented in Fig 9. It can be seen that presence of the particulate phase results in an overall retardation of the gas phase in the nozzle region. Further, the Mach number contours for the two-phase simulation also exhibit a distinct distortion, which is a consequence of a larger concentration of the particulate phase in this region. Parametric studies were carried out to investigate the effect of particle size on the two-phase flow-field by changing the particle size from 50 µm to 200 µm. The slag accumulation rates for different particle sizes are shown in Fig 10. The slag accumulation rate increases with the increase in particle size.

3.3 Slag Accumulation Prediction of Solid Rocket Motor for Strategic Applications

The validated methodology for single-phase and two-phase flows is applied to predict the slag accumulation in a practical solid rocket motor with submerged nozzle designed for strategic applications. The schematic of the rocket motor is shown in Fig. 11. Quasi-steady numerical solutions for six

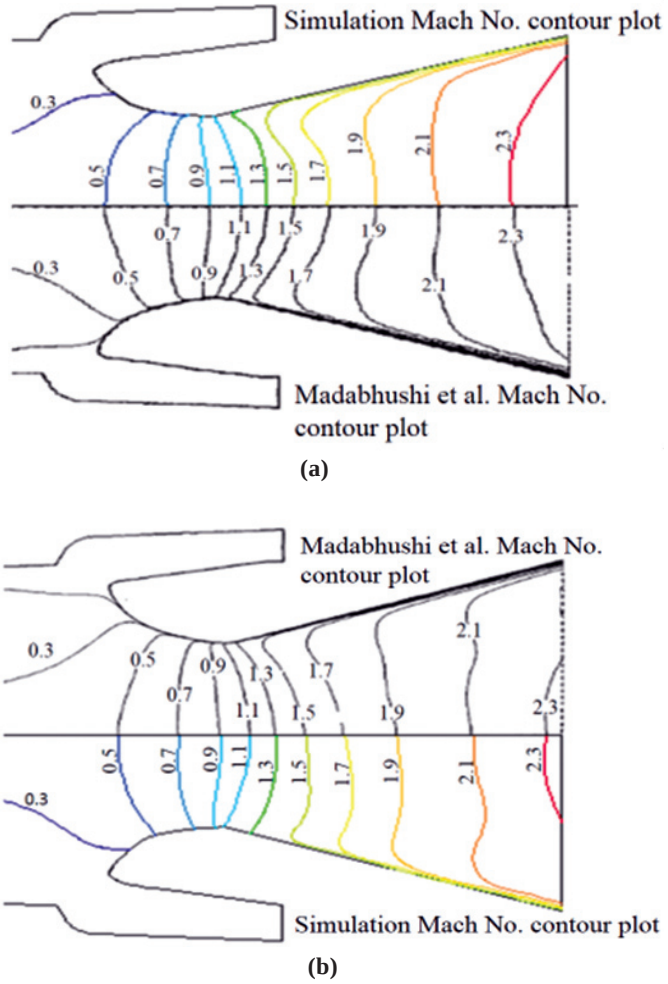

Figure 8. Mach number contour plots comparison with Madabhusi[24], *et al.*: (a) single-phase flow simulation, (b) two-phase flow simulation.

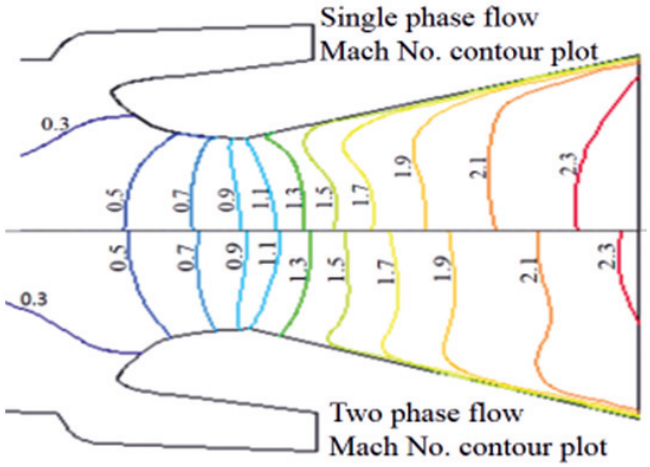

Figure 9. Comparison of single-phase and two-phase flow Mach numbers.

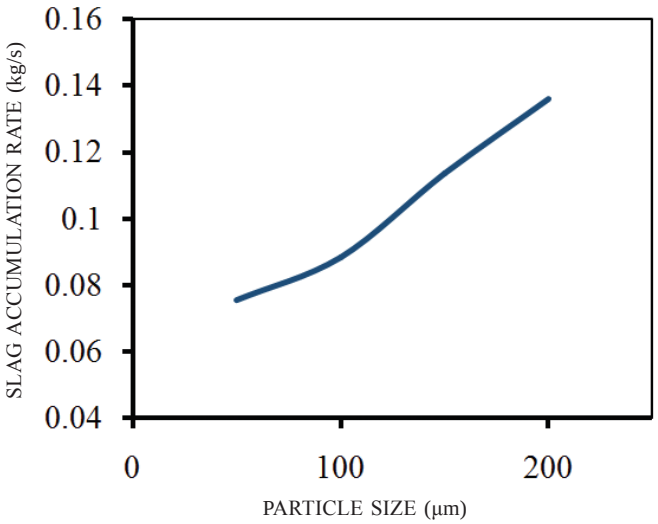

Figure 10. Slag accumulation rate for different particle sizes.

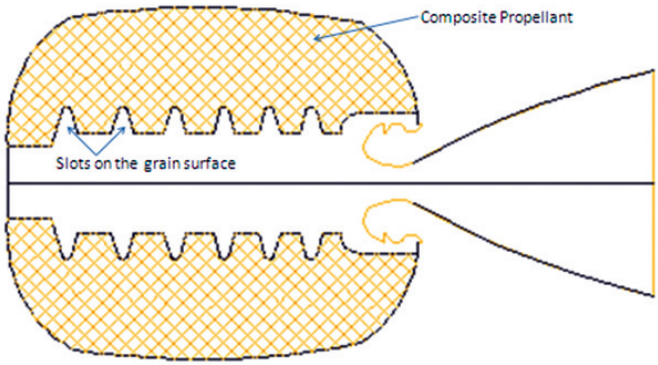

Figure 11. Practical motor along with propellant grain, nozzle, and motor casing.

burn-back geometries (0s, 10s, 20s, 30s, 40s, and 50s) that span the total burn time of 60 s and three different droplet sizes (20 μm, 50 μm, and 100 μm) have been considered. The solutions for the different burn-backs enable us to examine how the slag capture rate varies with time, and to predict the total amount of slag accumulation by integrating the slag capture rate over the total time. Six number of slots and the entire counter-bore is modelled along with the cavity region, radiation shield and the convergent-divergent nozzle. Axisymmetric analyses has been carried out for the entire burn duration. The mass flow rate for each time-step has been calculated from the ballistic program. The geometry for the flow-field simulation has been calculated from the regression pattern of the burning surface of the propellant. The different burn-back geometries are given in Fig. 12.

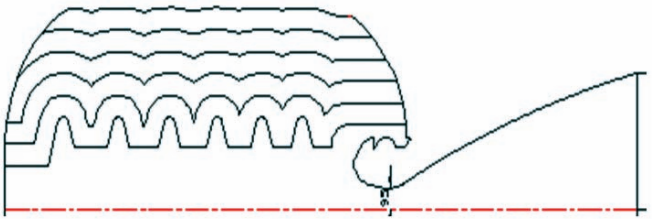

Figure 12. Different burn back geometries for flow simulations.

The internal geometry has been divided into 24 blocks to achieve the desired mesh profile. Total number of quadrilateral cells varies from 0.16 mm for 0s to 0.29 mm for 50s. Inert alumina (Al_2O_3) particles of different sizes (20 μm, 50 μm, and 100 μm) have been injected into the propellant surface along with the counter-bore region. The particles have been injected along with the continuous gas flow to simulate the two-phase flow condition and the alumina particles were made to interact with the continuous gas flow. The particle shape is assumed to be spherical, and also it does not change its shape during the flow. Quench bomb measurements[25] for a wide range of propellants suggest that particle size distributions are bimodal log-normal, with small (smoke) particles of mass-median diameter of roughly 1.5 μm, comprising 70-80 per cent of the particle mass, and the large-particle mode of mass-median diameters ranging from 20-100 μm, comprising only 20-30% of the mass. In the absence of any particle distribution pattern along the propellant geometry of the present motor, a fixed particle diameter is assumed in the present study and its effect is estimated for slag accumulation.

The qualitative feature of the flow behaviour in the nozzle is shown through the contours of static pressure in Fig. 13 for 10s burn-back geometry. The simulation captures all the essential features of the flow-field inside the motor port. The velocity at the nozzle exit is 2743 m/s which matches closely with the design value. Comparison of two-phase flow and single-phase flow Mach No. for 50 s burn back configuration is shown in Fig 14. There is slight shift of Mach number contours in upstream direction and the two-phase loss in the motor is not very significant. Streak lines at 10 s burn-back configuration are shown in Fig 15.

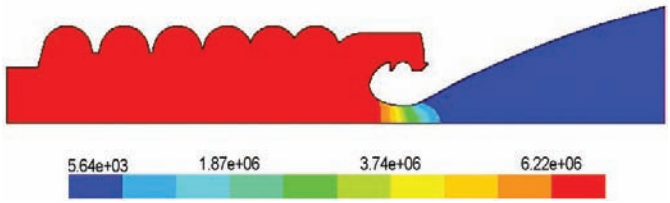

Figure 13. Contours of static pressure at 10 s.

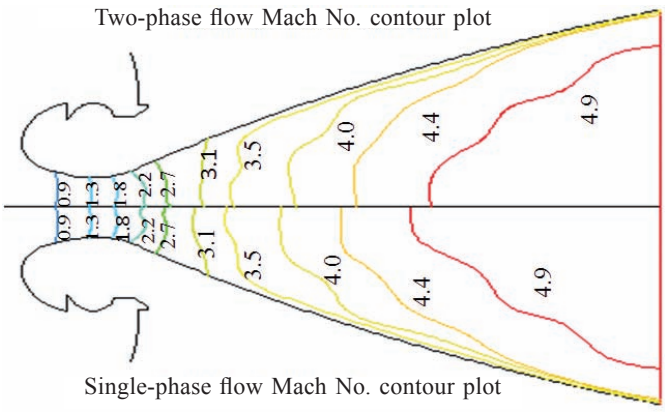

Figure 14. Comparison of two-phase and single-phase flow Mach numbers.

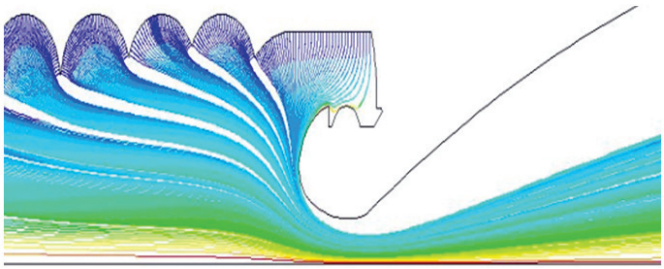

Figure 15. Streaklines in the flow at 10 s configuration.

The entire boundary of the flow domain in the submerged nozzle region is a burning surface at this time. The dominant feature of the flow-field in this region is the large-scale turning of the counter-bore flow towards the nozzle. It can be seen that droplet velocity vectors in cells adjacent to the nozzle wall have a component directed towards the wall; this indicates slag capture. Since a large entrance admits a larger amount of counter-bore flow into the cavity, which results in a large and faster turning flow, One would expect the slag capture rate to increase as the area of the cavity entrance increases.

Trajectories for different particle sizes at different burn-back configurations are analyzed which indicate that with increase in burn duration, the impingement of the particles at the backface of the nozzle increases and slag accumulation rate increases. Moreover, the contribution of the counter-bore region is seen to be more significant in the slag accumulation underneath the nozzle. Figure 16 shows the combined (20 µm, 50 µm and 100 µm) particle trajectories at 0s and 50s. It is observed that the particles captured underneath the nozzle are less at the starting of the motor firing, resulting in lower slag accumulation as compared to particles hitting the nozzle backface near the end of the motor firing, resulting in higher slag accumulation. The accumulated mass flow rates of the particles entering into the cavity for different particle diameters (20 µm, 50 µm, and 100 µm) obtained from simulations are presented in Fig. 17. The slag accumulation rate increases uniformly with droplet size for all burn-back times. With larger size of the particles, the accumulation rate is significantly higher. It is observed that between 50 µm and 100 µm size, accumulation rate increases by 45 per cent. Slag accumulation mass at different times are calculated for three

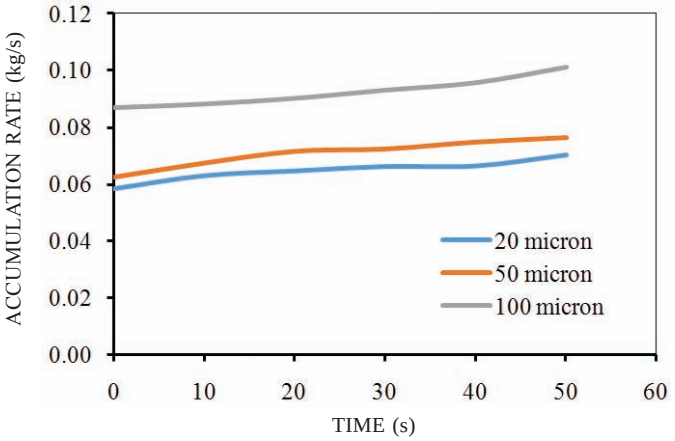

Figure 17. Slag accumulation rate at different instants of time.

Table 1. Slag mass at different times for different particle sizes

Time(s)	Non dimensional slag mass (Mslagmass/MAl)		
	20 µm particle	50 µm particle	100 µm particle
10	0.00038	0.00041	0.00055
20	0.0004	0.00044	0.00056
30	0.00041	0.00045	0.00058
40	0.00042	0.00046	0.0006
50	0.00043	0.00048	0.00062

droplet sizes and are presented in Table 1. The computed total non-dimensional slag mass accumulated (non- dimensionalised with aluminium mass) of this practical solid rocket motor is found to be 7.2×10^{-3} which matches closely with the measured non-dimensional slag mass (6.75×10^{-3} and 7.1×10^{-3}) in the two static tests of this rocket motor.

4. CONCLUDING REMARKS

Numerical simulations of the solid rocket motor port are carried out by performing both single-phase and two-phase flow analyses. Three-dimensional Navier-Stokes equations along with shear stress transport turbulence model are solved for gas phase calculations. The effect of ejected alumina particles from the propellant geometry on the flow-field is simulated through

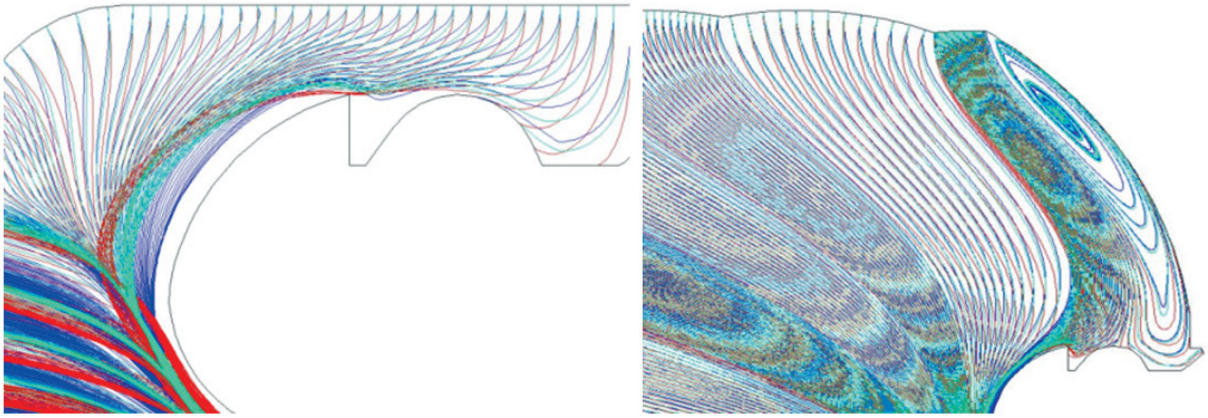

Figure 16. Combined (20 µm, 50 µm, and 100 µm) particle trajectories at 0 s and 50 s (Blue, green and red colours represents 20 µm,50 µm, and 100 µm particles, respectively).

Lagrangian tracking method. The computational methodology is validated by comparing the results with the numerical results of Titan IV SRMU and Space Shuttle RSRM motors reported in the literature. The computed axial distribution of centre line Mach number as well as the pressure ratio matches reasonably well with the literature values found in. The validated methodology is applied to predict the slag accumulation of a practical rocket motor for strategic applications. The flow-fields of different burn-back geometries at different instants were simulated and the effects of different particle trajectories on slag accumulation were evaluated. It is observed that:

- The rate of slag capture is approximately constant during the burn, prior to motor tail-off
- The onboard slag mass and the depth of the slag pool increase linearly with time, and
- The slag capture rate increases uniformly with $A1_2O_3$ droplet size. The predicted slag accumulation data match closely with the ground test data.

REFERENCES

1. Woodward Waesche, R. H.; Sargentt, William H. & Marchman III, J. F. Space shuttle solid rocket motor aft-end internal flows. *J. Propul. Power*, 1989, **5**(6), 650-656. Doi: 10.2514/3.23202
2. Caveny, L. H. Alon gany breakup of $A1/A1_2O_3$ agglomerates in accelerating flow-fields. *AIAA J.*, 1979, **17**(12), 1368-1371. Doi: 10.2514/3.7633
3. Salita, M.; Smith-Kent, R.; Golafshani, M.; Loh, H.-T; Abel, R. & Pratt, D. Prediction of Slag Accumulation in SICBM Static and Flight Motors. Thiokol TWR40259, Sept. 1990.
4. Salita, M. quench bomb investigation of AI_20_3 formation from solid rocket propellants (pt 11): analyses of data, 25th JANNAF Combustion Meeting, October 1988.
5. Salita, M. Deficiencies and requirements in modeling of slag generation in solid rocket motors. *J. Propul. Power*, 1995, **11**(1), 10-23. Doi: 10.2514/3.23835
6. Salita, M. unanticipated problems and misunderstood phenomena in and around solid rockets, *AIAA J.*, 2011, 5956. Doi: 10.2514/6.2011-5956
7. Cesco, N.; Dumas, L.; Hulin, A.; Pevergne, T. & Fabignon, Y. Stochastic models to the investigation of slag accumulation in a large solid rocket motor, *AIAA J.* 1997, 3118. Doi: 10.2514/6.1997-3118
8. Rosenband, V. & Gany, A. Agglomeration and ignition of aluminum particles coated by nickel. *Int. J. Energ. Mater. Chem. Propul.*, 2007, **6**(2), 143-152. Doi: 10.1615/IntJEnergeticMaterialsChemProp.v6.i2.10
9. Sippel, Travis R.; Son, Steven F. & Groven, Lori J. Aluminum agglomeration reduction in a composite propellant using tailored Al/PTFE particles. *Combust. Flame*, 2014, **161**(1), 311-32. Doi: 10.1016/j. combustflame.2013.08.009
10. Wn, X.; Aroro,R.; Knniar, M.; & Kilo, K. K. An aero-thermochemical model for erosive burning of double-base propellants in turbulent shear Flow. *In* Proceedings of the 13th international symposium on Space Technology and Science, Tokyo, June 28-July 2, 1982, 131-141.
11. King, M. K. A Model for prediction of effects of pressure, cross-flow velocity and heat of explosion on double- base propellant burning rate. *AIAA J.*, 1981, 81-1555. Doi: 10.2514/6.1981-1555
12. Beddini, R. A. Aero-thermochemical analyses of erosive burning in a laboratory solid rocket motor, *AIAA J.*, 1980, **18**(11), pp. 1340-1353. Doi: 10.2514/3.50890
13. Sabnis, J.S.; Giebeling, H.J. & McDonald, H. Navier-Stokes Analyses of Solid Propellant Rocket Motor Internal Flows. *J. Propul. Power*, 1989, **5**(6), 657-664. Doi: 10.2514/3.23203
14. De Jong, F.J.; Sabnis, J.S. & McConnaughey, P.K. A combined eulerian-lagrangian two-phase flow analyses of SSME HPOTP nozzle plug trajectories; pt I methodology. *AIAA J.*, 1989, 89-2347. Doi: 10.2514/6.1989-2347
15. Wirzberger, H.; Macales, Y.; & Yaniv, S. Prediction of slag formation in a solid rocket motor. *AIAA J.*, 2005, 4488. Doi: 10.2514/6.2005-4488
16. Najjar, F.M.; Haselbacher, A.; Balachandar, S.; Moser, R.D. Simulations of droplet nozzle impact and slag accumulation in the RSRM. *AIAA J.*, 2006, 4588. Doi: 10.2514/6.2006-4588
17. User Manual, Ansys, 2013.
18. Menter F.R. Two-equation eddy-viscosity turbulence models for engineering applications, *AIAA J.*, 1994, 32, 1598-1605. Doi: 10.2514/3.12149
19. Johnston, W.A.; Murdock, J.W.; Koshigoe, S. & Than, P.T. Slag Accumulation in the Titan SRMU. *AIAA J.*, 1994, 3487. Doi: 10.2514/6.1994-3287
20. Chang, I.-S. An efficient intelligent solution for viscous flows inside solid rocket motors, *AIAA J.*, 1991, 2429. Doi: 10.2514/6.1991-2429
21. Roache, P. J. verification and validation in computational science and engineering. Hermon Publishers, New Mexico, 1998.
22. Aswin, G. & Chakraborty, D. Numerical simulation of transverse side jet inter-action with supersonic free stream, *J. Aerosp. Sci. Techno.*, **14**(5), 295-301. Doi: 10.1016/j. ast.2010.02.001
23. Manna, P.; Dharavath, M.; Sinha, P.K. & Chakraborty, D. Optimization of a flight-worthy scramjet combustor through CFD. *J. Aerosp. Sci. Techno.*, 2013, **27**(1), 138-146. Doi: 10.1016/j.ast.2012.07.005
24. Madabhushi, R.K.; Sabnis, J.S.; De Jong, F.J. & Gibeling, H.J. Calculation of the two-phase aft-dome flow-field in solid rocket motors. *J. Propul. Power*, 1991, **7**(2), 178-184. Doi: 10.2514/3.23310
25. Jeenu, R.; Kiran, P. & Deepak, D. size distribution of particles in combustion products of aluminized composite propellan. *J. Propul. Power*, 2010, **26**(4), 715-723. Doi: 10.2514/1.43482

CONTRIBUTORS

Mr Amit Kumar Chaturvedi received his BTech in Aerospace Engineering from Aeronautical Society of India in 2001 and MTech in Aerospace Engineering from Indian Institute of Technology, Bombay, Mumbai, India in, 2013. He is working as a scientist at the Advanced systems Laboratory, DRDO, Ministry of Defence. His current research interests are in the areas of solid rocket propulsion, internal and two-phase flows. He is a member of Aeronautical Society of India. He has presented 5 research papers in national conferences.

Prof. Sudarshan Kumar is currently working as an Associate Professor in the department of Aerospace Engineering, Indian Institute of Technology Bombay. He has received his Master's and PhD degree in Aerospace Engineering from Indian Institute of Science, Bengaluru. His main areas of research include, microcombustion, flameless combustion, combustion instabilities in solid rockets, and gas turbine engines, emission reduction from combustion systems and modelling of combustion systems. He has more than 45 research papers published in various reputed international journals and more than 70 papers in various national and international conferences.

Dr Debasis Chakraborty obtained his PhD in Aerospace Engineering from IISc, Bengaluru. Presently, he is working as Technology Director, Computational Dynamics Directorate, DRDL, Hyderabad. His research interests include CFD, aerodynamics, high speed combustion, and propulsion. He has more than 60 journal papers and 80 conference publications to his credit.